Reprinted from MONTHLY WEATHER REVIEW, Vol. 124, No. 5, May 1996
American Meteorological Society

The Use of Surface Observations in Four-Dimensional Data Assimilation Using a Mesoscale Model

FRANK H. RUGGIERO

Atmospheric Sciences Division, Phillips Laboratory, Hanscom AFB, Massachusetts

KEITH D. SASHEGYI AND RANGARAO V. MADALA

Remote Sensing Division, Naval Research Laboratory, Washington, D.C.

SETHU RAMAN

Department of Marine, Earth, and Atmospheric Sciences, North Carolina State University, Raleigh, North Carolina

(Manuscript received 23 January 1995, in final form 12 October 1995)

ABSTRACT

A system for the frequent intermittent assimilation of surface observations into a mesoscale model is described. The assimilation begins by transforming the surface observations to model coordinates. Next, the lowest-level model fields of potential temperature, relative humidity, u and v component winds, and surface pressure are updated by an objective analysis using the successive correction approach. The deviations of the analysis from the first guess at the lowest model layer are then used to adjust the other model layers within the planetary boundary layer. The PBL adjustment is carried out by using the model's values of eddy diffusivity, which are nudged to reflect the updated conditions, to determine the influence of the lowest-layer deviations on the other model layers. Results from a case study indicate that the frequent intermittent assimilation of surface data can provide superior mesoscale analyses and forecasts compared to assimilation of synoptic data only. The inclusion of the PBL adjustment procedure is an important part of generating the better forecasts. Extrapolation of the results here suggests that two-dimensional data can be successfully assimilated into a model provided there is a mechanism to smoothly blend the data into the third dimension.

1. Introduction

Recently, increased focus has been put on the operational applicability of mesoscale analysis and forecast systems. Advances in computer technology make it possible that in the next few years mesoscale models ($\Delta x \approx 15-30$ km) will be routinely run at local forecast offices (Warner and Seaman 1990; Cotton et al. 1994). These models will be used to generate spatially and temporally detailed forecasts in the 3–36-h range. The models can be expected to have their own data assimilation system using centrally prepared forecasts and analyses only for the outermost horizontal boundary conditions. This local forecast office configuration of the near future raises two important questions. First, will the forecasters want to rely on a model that is only initialized at the synoptic times of 0000 and 1200 UTC (when radiosonde data is available). If forecasters are expected to produce highly accurate 3–6-h forecasts, it will be necessary to assimilate data into the model more often than twice a day. The second question is whether the current network of radiosonde observations is the best source of data for the increasingly high-resolution mesoscale models. As technology advances, there are a host of new data sources to be tapped. These data sources include automated surface observation systems, Doppler radars and wind profilers, automated aircraft reports, and increasingly sophisticated spaceborne sensors, which can provide high spatial and/or temporal resolution in limited regions.

Since its introduction by Charney et al. (1969), four-dimensional data assimilation (FDDA) has become the standard method of producing analyses for the initialization of global and regional models (Daley 1991; Harms et al. 1992a). FDDA involves using the temporal evolution of fields of meteorological variables in combination with a numerical weather prediction model to provide enhanced meteorological analysis. This enhanced analysis is then used for model initialization or a detailed diagnostic dataset. A typical procedure for an operational assimilation system is that used by the National Meteorological Center's (NMC) Global Data Assimilation System, which assimilates new data every 6 h at the usual synoptic hours of 0000

Corresponding author address: Frank H. Ruggiero, Naval Research Laboratory, Code 7225, 4555 Overlook Avenue SW, Washington, DC 20375-5000.
E-mail: ruggiero@atmos.nrl.navy.mil

and 1200 UTC and at the asynoptic hours of 0600 and 1800 UTC (Kanamitsu 1989).

In preparation for new high-frequency observation systems, research has been carried out to simulate the impact of the more frequent assimilation of asynoptic data on limited-area models. Harms et al. (1992b) used intermittent assimilation of the frequent upper-air data that were available during the Genesis of Atlantic Lows Experiment (GALE). During GALE, upper-air radiosonde soundings were available every 3 h during intensive observation periods (IOP). In addition, the spatial coverage was increased over the eastern Carolinas and the adjacent Atlantic Ocean. The results showed that the analyses created during the assimilation were superior to those available from the Regional Analysis and Forecast System (RAFS) analysis, particularly with respect to accurately defining mesoscale features. Stauffer and Seaman (1990) used temporally interpolated NMC analyses to simulate frequent asynoptic wind and thermodynamic observations. These data were assimilated by Newtonian nudging and resulted in analyses that accurately produced meteorological features on a scale smaller than the spatial resolution of the assimilated data. Although these first studies of asynoptic data assimilation were successful, they did have the advantage of either using or simulating three-dimensional data that contained both mass and wind fields. In reality most of the new data sources are not as ideal. Manobianco et al. (1991), for example, used a nudging method to assimilate the special 3-h soundings and surface data from GALE IOP 10 with limited success in improving forecasts produced with a limited-area model.

Research has been ongoing at the National Oceanic and Atmospheric Administration's Forecast Systems Laboratory to develop assimilation systems for the meso- (Benjamin et al. 1991) and local scales (McGinley et al. 1991; Snook et al. 1994). These systems rely heavily on asynoptic data sources and use short assimilation cycles. This work has led to the operational installation at NMC of the Rapid Update Cycle (Benjamin et al. 1994), which assimilates in real time 3-h asynoptic data. In addition, NMC also uses 3-h asynoptic data in the off-line assimilation that is run in the 12 h before the Nested Grid Model's initialization (DiMego et al. 1992).

Currently, hourly surface observations are one of the most abundant sources of asynoptic data. Miller and Benjamin (1992) describe a system for the assimilation of surface data that uses a 1-h persistence forecast as the background to produce a detailed mesoscale analysis. The current average spatial resolution of hourly surface reporting stations in the United States is approximately 80 km as opposed to about 350 km for radiosonde stations. This will soon be augmented by the deployment of the Automated Surface Observing Systems to airports where observations are currently not available (Friday 1994). In addition, several areas of the country are also served by automated surface mesonets. Assimilating hourly surface data into a model should yield a better planetary boundary layer (PBL) forecast due to the more-frequent boundary forcing by the surface data. Better PBL representation is important because a large number of forecast requirements are within the boundary layer. Although surface data do not produce direct observations of the upper air, Yee and Jackson (1988) have outlined a scheme where differences between surface observations and the bottom layer model forecast can be used to adjust the other model layers.

This paper will describe a system for the asynoptic assimilation of hourly surface observations into the limited-area model from the Navy's Operational Regional Atmospheric Prediction System (NORAPS). This is part of a larger research effort to produce a prediction and analysis system for local forecast office use that is efficient enough to work on a high-performance workstation and yet sophisticated enough to produce useful and accurate short-term forecasts. In this study, the impact of the surface observations on the objective analysis and model forecasts will be examined. In addition to using the surface data to modify the lowest level of the model fields, a physically based technique will be described that adjusts model layers within the PBL on the basis of the deviations of the surface analysis from the forecast model's lowest layer. Because surface observations are but one important asynoptic data source, what is learned here might also be useful in assimilating other asynoptic data sources.

2. Assimilation system description

a. Assimilation method

The limited-area modeling system developed here follows the form of intermittent assimilation. A flowchart detailing how the intermittent assimilation works is given in Fig. 1. Intermittent assimilation combines in an objective analysis a set of observa-

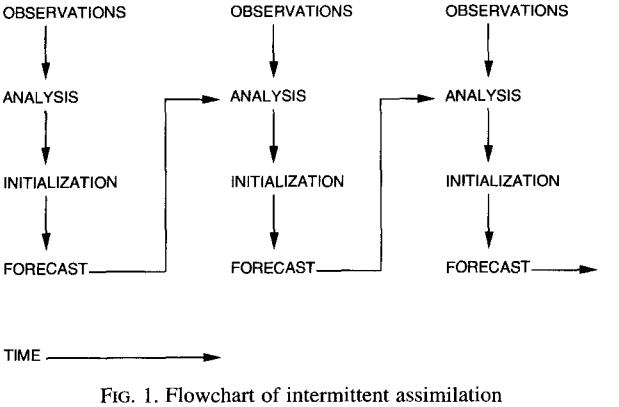

FIG. 1. Flowchart of intermittent assimilation analysis–forecast stream.

tions with a short-term forecast valid at the same time. The new analysis is run through a model initialization step before being used to generate the next set of forecasts. Admittedly, intermittent assimilation does not represent the most advanced FDDA method, but it does satisfy the constraint that the limited-area assimilation system must work quickly on a high-performance workstation. Advanced FDDA techniques such as the adjoint and Kalman–Bucy filter are very computer intensive and will probably remain in the realm of major forecast centers and large mainframe computers for the near future. The advantages of intermittent assimilation are that it is efficient and relatively easy to implement. Another important attribute of analyses and forecasts produced by intermittent assimilation is that the meteorological inconsequential fast-mode gravity waves in the initial conditions can be significantly reduced when the mass and wind fields are balanced by the application of a normal mode initialization scheme for the limited-area model (Bourke and McGregor 1983). This lessens the chance that the model will be shocked by unbalanced new data, an important consideration, particularly in the first 6 or 12 h of integration using a limited-area forecast model. Walko et al. (1989) illustrated what can happen when nudging the prognostic equations toward wind observations. After a period of assimilation, the assimilated wind field was rejected by the model because of the generated imbalance between mass and wind fields. For longer forecasts (>12 h), the gravity wave noise can be removed by the imposed damping that occurs in the lateral boundary regions of the limited-area models. There may be some disadvantages, however, of having to perform an initialization every time new data are assimilated. The main one is that the divergent portion of the wind generated by the model may be removed if the analysis corrections are large or there are substantial differences in diabatic heating generated by the model and that used by the initialization scheme. Thus, how frequently the assimilation cycle should be applied is open to subjective judgment. Another potential problem with intermittent assimilation of asynoptic surface data (or any other single-level data) is that the initialization can reject some of the features added to the analysis by the observations. This could occur if the assimilated surface data deviated substantially from the first guess provided by the model forecast. The initialization would see discontinuities between the model's lower levels and could perceive them as gravity waves and damp the surface deviations out. Barwell and Lorenc (1985) showed this to be a cause of the limited retention of assimilated single-level aircraft wind data in subsequent forecasts. For this reason, an attempt is made in the analysis to adjust layers above the model's lowest layer.

b. *Forecast model*

The model used in this assimilation system is NORAPS version 6 (Liou et al. 1994). This is the latest version of the model that has been previously described by Madala et al. (1987), Hodur (1987), and Liou et al. (1990). NORAPS is currently run operationally by the U.S. Navy Fleet Numerical Meteorological and Oceanography Center for several areas of the world on a CRAY C90 supercomputer. Work is underway to port the model to a high-performance workstation. Initial tests on a RISC-type workstation with a floating point performance of 30 Mflops using a simplified configuration of the model have produced a 12-h model forecast in approximately 30 min (Sashegyi et al. 1994). NORAPS is a hydrostatic, primitive equation model written in flux form. The spatial finite difference equations are fourth-order accurate in the horizontal and second-order accurate in the vertical. Time integration is done using the efficient split-explicit scheme of Madala (1981). A Robert (1966) time filter is used to control high-frequency time oscillations. NORAPS contains a Kuo (1974) parameterization for deep convection and follows the approach of Tiedtke et al. (1988) for shallow convection. Large-scale precipitation is produced after the cumulus parameterization has been run by isobarically condensing of regions of supersaturation following the procedure of Manabe et al. (1965). Precipitation falling into unsaturated layers is evaporated. A multilevel planetary boundary layer is solved using similarity theory in the surface layer following Louis (1979) and vertical turbulent mixing above it. The mixing is accomplished by turbulent kinetic energy closure (Detering and Etling 1985). Surface temperatures are obtained from surface energy budget considerations using a two-layer force–restore method (Blackadar 1979). Atmospheric heating due to longwave and shortwave radiation is updated every hour following the approach of Harshvardhan et al. (1987).

The horizontal grid is a staggered Arakawa C grid (Arakawa and Lamb 1977). The model is triple nested with the lateral boundary time tendencies for the outer grid relaxed toward interpolated global analysis and forecast time tendencies by the method of Perkey and Kreitzberg (1976). For the inner grids, the values of the variables on the two grids are merged using the Davies (1976) method.

c. *Upper-air analysis*

The objective analysis of the upper-air data is accomplished by the successive correction scheme of Bratseth (1986) as adapted by Sashegyi et al. (1993). One advantage of this scheme is that although the analysis will converge to the optimum interpolation solution, it requires less computer time and memory. Thus, it is well suited for implementation on a high-perfor-

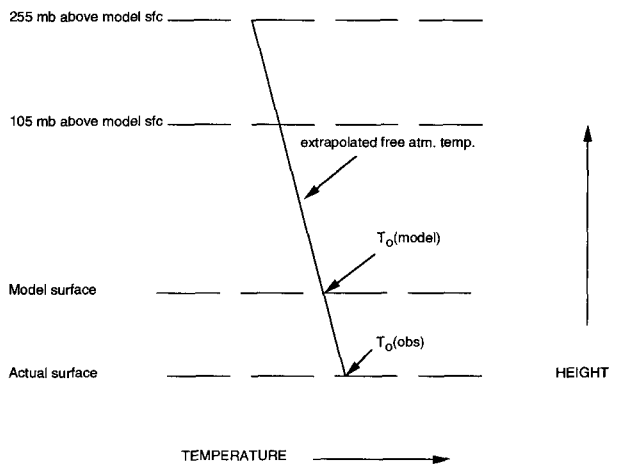

FIG. 2. Schematic of T_0 calculation for sea level pressure reduction.

mance workstation. The Bratseth analysis scheme also avoids the limitation previous successive correction methods had of converging to observations and giving too much weight to observations in data-dense regions. Upper-air observations are analyzed on every 50-mb surface from 100 to 1000 mb using a horizontal spatial resolution of 1.5° in latitude and longitude. At the synoptic hours, bogus soundings derived from operational analyses for a larger domain regional or global model are added to fill in data-sparse regions over the ocean. The deviations from the first guess are then vertically interpolated back to the sigma surfaces. Extrapolation is used for sigma surfaces below 1000 mb. For the regions of the model grid that lie outside the analysis domain, the analysis corrections are computed by interpolation from the operational larger domain analysis at the synoptic hours, whereas the analysis reverts to the background field at the asynoptic hours.

d. Surface data analysis

At synoptic and asynoptic hours the bottom model level variables of pressure, temperature, moisture, and winds are updated by a modified version of the Sashegyi et al. (1993) analysis using surface observations only.

1) TRANSFORMATION OF SURFACE DATA TO MODEL COORDINATES

The lowest sigma layer is $\sigma = 0.9975$ and is approximately 20 m above the model's surface. The surface variables are typically measured at heights between 1.5 and 10 m above ground level. Differences of altitude above mean sea level between the observations and the lowest model sigma layer can also arise. This occurs because of the finite horizontal resolution of the model's topography. Therefore, it is important to take out any altitude bias from the differences of the observations to the model background. For surface pressure, this is accomplished by reducing the model and observed surface pressures to sea level. The analysis is done using the sea level pressures and then converted back to surface pressure on the model topography. The conversion to and from sea level pressure is done using the following standard equation:

$$p_{sl} = p_{sfc}\left(\frac{T_0 + \gamma z}{T_0}\right)^{g/\gamma R}, \qquad (1)$$

where p_{sl} and p_{sfc} are the sea level and surface pressures, respectively, γ is the standard lapse rate, R is the dry gas constant, g is the gravitational constant, and T_0 is the effective virtual temperature at the top of a fictitious column of air that lies between the surface and sea level. Following a variation of the procedure of Benjamin and Miller (1990), the upper-air data provided by the model background field is used to determine a T_0 that is free of any boundary layer influences. A schematic showing how T_0 is derived is given in Fig. 2. This is done by determining an atmospheric lapse rate using virtual temperatures at 105 and 255 mb above the model's surface from the background data. The levels of 105 and 255 mb above the surface were chosen to ensure that the lapse rate was calculated above the PBL. The lapse rate is then used to extrapolate the temperature at 105 mb above the surface down to the surface of either the model or observation. The observation and background may have slightly different T_0 values. This is due to the differences in elevation of the observations and the model's surface.

For the surface temperature, the analysis is carried out using the deviation of observed surface potential temperature from the potential temperature extrapolated from a mean profile. A schematic of how the potential temperature deviations are arrived at is shown in Fig. 3. The mean potential temperature profile is de-

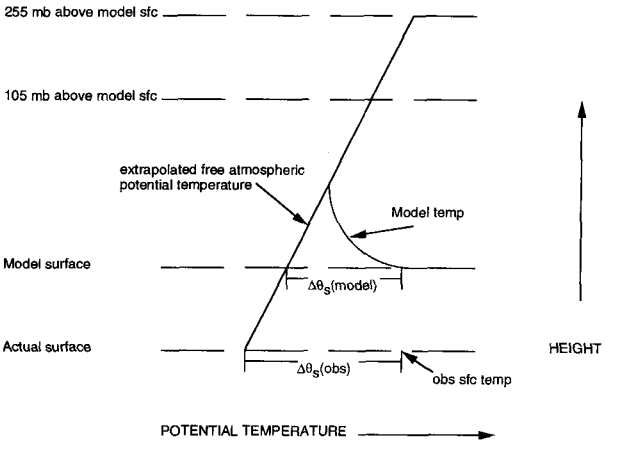

FIG. 3. Schematic of surface potential temperature deviation estimation.

termined by using the free atmospheric potential temperature lapse rate in the same manner as described above. The profile extends from the model potential temperature at 105 mb above the model's surface down to both the model's lowest sigma layer and the observation height. The deviations of the model surface potential temperature from that of the extrapolated mean profile, $\Delta\theta_s(\text{model})$, form the background field of the analysis. The differences between the observed potential temperature and the corresponding extrapolated potential temperature from the mean profile, $\Delta\theta_s(\text{obs})$, are the analyzed variables. In the diagram in Fig. 3, although the observed and model potential temperatures are the same, the deviation of the observed surface potential temperature is larger than the deviation computed from the model's lowest layer. The observation indicates more surface heating than the model when taking into account the altitude difference between the model and observation surfaces. By analyzing the deviations from the mean potential temperature profile, differences due to altitude are minimized. When the analysis is complete, the analyzed differences are then added back to the potential temperature from the mean profile corresponding to the lowest model level.

Because moisture varies with altitude mainly because of temperature and pressure, the moisture analysis is conducted using relative humidity as opposed to mixing ratio. Winds generally do not behave as a function of absolute elevation, but as a function of height above the surface. However, the difference above ground level between model height and observation height is generally only about 10 m. A height transformation for the horizontal wind suitable for all stability categories does not exist. Therefore, no altitude adjustments for winds have been attempted.

2) OBJECTIVE ANALYSIS

The objective analysis for the surface data is similar to that used for the upper-air data. The analysis procedure of Sashegyi et al. (1993) was adapted to take advantage of the increased resolution of the surface data. The analysis was performed on a domain the same as the upper-air analysis but with the resolution set at 0.5° latitude and longitude to account for the increased data density of surface observations. Observations within 0.33° latitude and 0.41° longitude of each other are averaged to form superobs. Univariate analyses are conducted for sea level pressure and potential temperature deviations, relative humidity, and u and v wind components on the lowest model sigma layer. The successive correction method works in an iterative fashion updating the background fields using the difference between the observed values and observational estimates derived from the analysis. At a grid point x, the updated analysis value for the u component wind is given by

$$u_x(k+1) = u_x(k) + \sum_{j=1}^{n} \alpha_{xj}[u_j^o - u_j(k)], \quad (2)$$

where $u_x(k)$ is the analysis value at a grid point at the kth iteration, u_j^o is the observation at the jth station, $u_j(k)$ is the observational estimate at the jth station and kth iteration, n is the total number of observations that influence a particular grid point, and α_{xj} is the weighting function between the jth observation and the grid point x. The weights contain functions that spatially correlate observation and analysis locations with themselves and each other (Bratseth 1986). The correlation functions used for sea level pressure, potential temperature, relative humidity, and horizontal winds were the same as those used by Miller and Benjamin (1992) in their optimal interpolation analysis. The functions follow a basic Gaussian form with additional terms included to account for differences in terrain elevation for potential temperature and potential temperature gradients for winds and humidity. Instead of using a polynomial interpolation of the updated analysis to calculate a new value of the observational estimate, the same interpolating formula as Eq. (2) is used in the Bratseth scheme,

$$u_i(k+1) = u_i(k) + \sum_{j=1}^{n} \alpha_{ij}[u_j^o - u_j(k)], \quad (3)$$

where $u_j(k)$ is the observational estimate at the ith observation location for the kth iteration. The main difference between Eqs. (2) and (3) lies in the definition of the weights. The weights used to compute the observation estimates contain an additional term that accounts for observational error. This has the practical effect of allowing the observational estimate to converge more quickly to the observation values than the analysis. The error function included in the observation estimate weighting function is defined as the ratio of the observation error variance to the first-guess error variance. The first-guess error standard deviation is estimated by summing the standard deviation of the observational error and forecast error growth (Sashegyi et al. 1993). The observation error standard deviations and forecast error growth rates used for in this study are given in Table 1. Selection of the error values is important in the analysis to determine the closeness of fit of the analysis to the observations. Ideally, the values chosen should be based on a large sample of the model and observations. In a research mode this is usually impossible. The values used here are generally based

TABLE 1. Standard deviation of the observational errors and the forecast error growth rates for a 6-h forecast period.

Field	Observation error	6-h forecast error growth rate
Sea level pressure (mb)	1.5	1.0
Potential temperature (K)	2.5	2.5
Relative humidity (%)	13	2
u, v wind (m s^{-1})	2.5	1.1

on values used at NMC for the RAFS analysis (DiMego 1988). Trial and error testing of the analysis were carried out to check if the values chosen were suitable. This led to an increase in both the observation error and forecast error growth for the surface potential temperature analysis. In addition, the ratio of observed-to-forecast error for potential temperature was increased. After the set of experiments described in section 3 were completed, the standard deviations of the observations from the model forecast were compared to ensure that they generally fit within the specifications in Table 1. For the surface data analyses at asynoptic times the model forecast valid at that time serves as the background field for the analysis and $u_x(1)$ and $u_i(1)$ are set to zero. At 0000 and 1200 UTC the analysis of the upper-air data is done first, and that result serves as the first iteration in the surface data analysis and observational estimates. The analysis proceeds using the model forecast as the background field and continues for four to five iterations as was used in the upper-air analysis (Sashegyi et al. 1993).

3) PBL ADJUSTMENT

Unique to this assimilation system is a procedure that modifies model fields above the lowest layer on the basis of deviations between the surface observations and the background field. The reason for putting in the adjustment procedure is to have a smooth transition from the lowest model layer analysis to the rest of the model. This provides the subsequent initialization procedure with a more vertically consistent set of fields so that it retains more of the deviations from the analysis. Benjamin (1989) was able to vertically distribute the influence of surface observations by performing the analysis on isentropic surfaces. The procedure described here is carried out on pressure surfaces and is an outgrowth of the work by Yee and Jackson (1988), who described how one might blend surface data with radiosonde data. They postulated that the deviations of the observations from the background at the surface could be used to influence the background levels above the surface. For their testing, Yee and Jackson (1988) used a simple linear weighting function as the influence function. However, they saw the need for a more physically based function. For this effort an adjustment procedure based on parameterized values from the heat and momentum fluxes from the background fields was developed. The derivation of the adjustment procedure is illustrated by looking at the adjustment procedure for temperature. Starting with the equation for the conservation of heat in turbulent flow (e.g., Stull 1988),

$$\frac{\partial\bar{\theta}}{\partial t}+\bar{u}\frac{\partial\bar{\theta}}{\partial x}+\bar{v}\frac{\partial\bar{\theta}}{\partial y}+\bar{w}\frac{\partial\bar{\theta}}{\partial z}=-\frac{1}{\bar{\rho}C_p}\times\left(L_vE+\frac{\partial\bar{Q}_*}{\partial x}+\frac{\partial\bar{Q}_*}{\partial y}+\frac{\partial\bar{Q}_*}{\partial z}\right)-\frac{\partial(\overline{w'\theta'})}{\partial z}. \quad (4)$$

Here θ is potential temperature, u, v, and w are the component winds, ρ is the density, C_p is the specific heat constant, L_v is the latent heat of the vaporization of water, E is the phase rate of change, Q_* is the component of net radiation, and $\overline{w'\theta'}$ is the turbulent heat flux. The heat flux can be parameterized by $-K_h[\partial(\bar{\theta})/\partial z]$ where K_h is the thermal vertical diffusion coefficient, which allows Eq. (4) to consist entirely of the mean quantities of variables and the overbar notation to be dropped. The next step is to separate these mean variables into background and analysis deviation components. In so doing, all the terms that consist solely of background terms can be deleted assuming the background is in balance. Thus, Eq. (4) becomes

$$\frac{\partial\theta_d}{\partial t}=-u_{bg}\frac{\partial\theta_d}{\partial x}-u_d\frac{\partial\theta_{bg}}{\partial x}-u_d\frac{\partial\theta_d}{\partial x}-v_{bg}\frac{\partial\theta_d}{\partial y}-v_d\frac{\partial\theta_{bg}}{\partial y}-v_d\frac{\partial\theta_d}{\partial y}-w_{bg}\frac{\partial\theta_d}{\partial z}-w_d\frac{\partial\theta_{bg}}{\partial z}-w_d\frac{\partial\theta_d}{\partial z}+\frac{\partial}{\partial z}K_h\frac{\partial\theta_d}{\partial z}. \quad (5)$$

The subscript bg denotes background terms and d the deviation terms. A scale analysis on the terms in Eq. (5) reveals that the tendency of θ_d and vertical diffusion terms are approximately two orders of magnitude larger than the other terms and Eq. (5) is simplified to

$$\frac{\partial\theta_d}{\partial t}=\frac{\partial}{\partial z}K_h\frac{\partial\theta_d}{\partial z}. \quad (6)$$

Likewise for the wind and moisture fields, the following can be derived:

$$\frac{\partial u_d}{\partial t}=\frac{\partial}{\partial z}K_m\frac{\partial u_d}{\partial z}, \quad (7)$$

$$\frac{\partial v_d}{\partial t}=\frac{\partial}{\partial z}K_m\frac{\partial v_d}{\partial z}, \quad (8)$$

$$\frac{\partial q_d}{\partial t}=\frac{\partial}{\partial z}K_h\frac{\partial q_d}{\partial z}. \quad (9)$$

Using these relationships, the adjustment procedure is used to solve for deviations from the background field above the lowest model layer by stepping forward in time. When solving the vertical system of equations, the deviation values at the lowest and highest model layers are held constant. At the top, the deviations are 0 and at the bottom the deviations are set by the surface data analysis. Equations (6)–(9) attempt to represent physically the vertical distribution of deviations caused by the surface-layer forcing. Implicit here is that the vertical propagation of the deviations will be restricted to the boundary layer. This is acceptable based on the scale analysis. Equations (6)–(9) are evaluated starting with the model's diffusion coefficients. After each iteration a new set of coefficients is calculated using

TABLE 2. Configuration of assimilation experiments.

Number	Upper-air updates (h)	Surface data updates (h)	PBL adjustment
1	12	—	No
2	12	12	No
3	12	12	Yes
4	12	6	Yes
5	12	3	Yes

the mixed layer approach (Blackadar 1979). The original diffusion coefficients are then nudged toward the new values following the approach of Stauffer and Seaman (1990). The coefficients are nudged instead of replaced because recalculating the coefficients completely in the beginning would lead to erroneous coefficient values. The new coefficients would be affected because of the discontinuity between the lowest sigma layer and those above. An example would be when the updated bottom sigma layer temperature is significantly cooler than the forecast. This could result in an extremely shallow stable layer and a new coefficient calculated for this layer would be near zero. This would shut down any cooling of the layers above. The idea in nudging the coefficients is that at the end of the PBL adjustment an equilibrium of the vertical momentum, thermodynamic, and eddy diffusivity values can be achieved. Because the model values of diffusion coefficients are based on turbulent kinetic energy and can contain some high-frequency noise, a light horizontal filter is passed over the deviations at each iteration of Eqs. (6)–(9). Because the lowest layer analysis deviation grows over the forecast period, the length of the forecast would then be the upper bound on how long to run the PBL adjustment. In application, however, care must be taken in how much one would want to infer changes above the surface in the absence of direct observations. If the adjustment is carried out too long, the result could be a strong vertical discontinuity at the top of the boundary layer instead of the lowest model layer. A time period of 30 min for performing the PBL adjustment was selected after experimentation.

e. Initialization

The assimilation system uses the nonlinear normal vertical mode initialization as described by Sashegyi and Madala (1993). The initialization procedure minimizes the time tendencies of the first three vertical (nonmeteorological) modes to reduce spurious oscillations caused by gravity waves. As described by Sashegyi and Madala (1993), the initialization is carried out without any boundary layer forcing or diabatic heating. For this adiabatic assimilation procedure a first-order closure mixing length PBL package was added to the physical forcing.

3. Experiment design

Data from GALE IOP 2 is used for the purpose of testing the assimilation system. GALE IOP 2 took place from 23 to 28 January 1986. Detailed accounts of the case can be found in Riordan (1990) and Doyle and Warner (1990). GALE IOP 2 began as a cold air damming event east of the Appalachian Mountains as surface high pressure moved eastward over eastern Canada. A coastal front formed over the west wall of the Gulf Stream between 1200 UTC 24 January and 0000 UTC 25 January. The coastal front moved slowly west and eventually came onshore into eastern North Carolina. By 0000 UTC 26 January a small low formed along the coastal baroclinic zone just off the South Carolina coast and moved northward. This had the effect of pulling the coastal front back to the east along the North Carolina coast.

Five experiments were run to assess the impact of surface data assimilation. The key features of each experiment are listed in Table 2 and a schematic delineating the assimilation and forecast periods is shown in Fig. 4. All the experiments start off with a 12-h run of the NORAPS model initialized at 1200 UTC 24 January 1986 using 2.5° RAFS hemispheric analysis fields. Experiment 1 assimilated upper-air data only at 0000 and 1200 UTC 25 January. Where radiosonde soundings were not available at 0000 and 1200 UTC, the RAFS hemispheric analysis fields are used to provide bogus soundings over the Atlantic and analysis corrections outside the analysis domain (see section 2c). Experiment 2 is the same as experiment 1 except that a surface data analysis was conducted after the upper-air analysis. The surface observations used included regularly reporting hourly stations, Portable Automated Mesonet System (PAMS) stations that were located in the eastern part of North and South Carolina during GALE, and marine ship and buoy reports. Experiment 3 is the same as experiment 2 except that after each

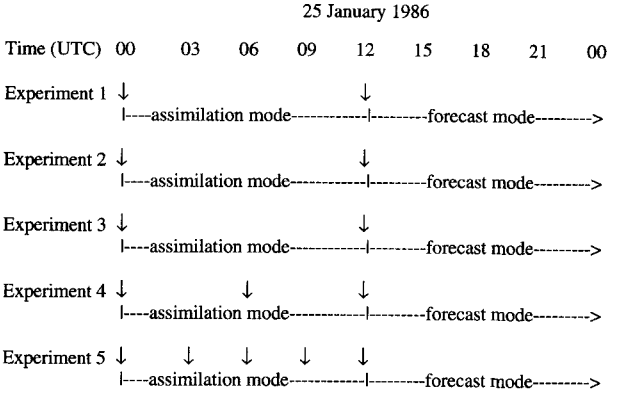

FIG. 4. Depiction of assimilation and forecast periods for the experiments in Table 2. The downward pointing arrows indicate times at which updates were performed.

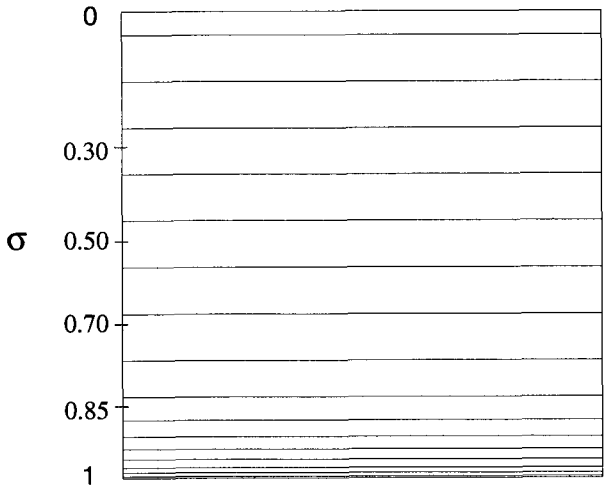

FIG. 5. Vertical distribution of the 16σ levels for NORAPS model configuration used in this study.

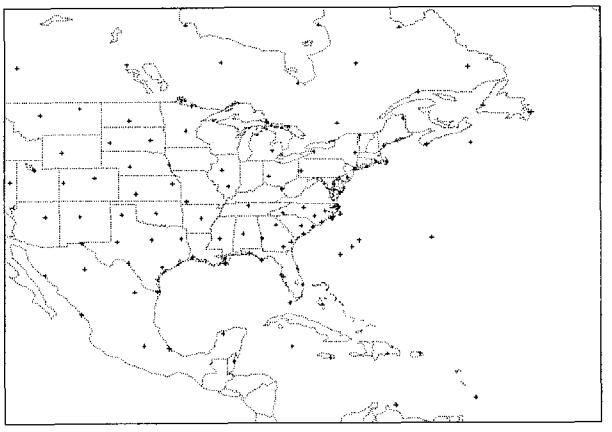

FIG. 7. Location of upper-air stations within the objective analysis domain reporting at 0000 UTC 25 January 1986.

surface data analysis, the PBL adjustment procedure was used to merge the surface data analysis with the upper-air analysis at model levels above the surface. Experiment 4 was similar to experiment 3 except that a 6- instead of 12-h assimilation cycle was used. At nonsynoptic hours only the surface data analysis and PBL adjustment procedure modifying the model first guess were run. Experiment 5 was the same as experiment 4 except a 3-h assimilation cycle was used. For all the experiments the model was run to 12 h without further assimilation from 1200 UTC 25 January. The purpose of this was to be able to gauge for how long the surface data assimilation can improve a forecast. For the experiments, the NORAPS model was run with 16 vertical terrain following sigma ($\sigma = p/p_s$) layers. The vertical resolution is depicted in Fig. 5. It is the same for all three grids and increases near the surface such that seven of the layers are below $\sigma = 0.85$. The domains of the three model grids used in this study are shown in Fig. 6. The horizontal resolution of the outermost grid was 2.0° longitude by 1.5° latitude, with each successive inner grid having a threefold increase of resolution over its outer grid. The innermost resolution was approximately 18 km. Interpolated RAFS analysis values were used for the horizontal boundary conditions of the outermost grid. The topography for the innermost grid was constructed from 10′ terrain data. Sea surface temperature data from the weekly 14-km AVHRR database were used as well as climatological seasonal albedo and sea ice information. The analysis domain for both upper-air and surface data is 10.0°–60.5°N, 115.5°–44.5°W. The domain is shown in Figs. 7 and 8 along with examples of the number and density of upper-air and surface reporting stations.

For the purposes of objective evaluation, the analyses and forecasts generated by the surface data assimilation are compared to the independent analyses presented by Doyle and Warner (1990). Doyle and Warner (1990, hereafter referred to as DW) constructed a

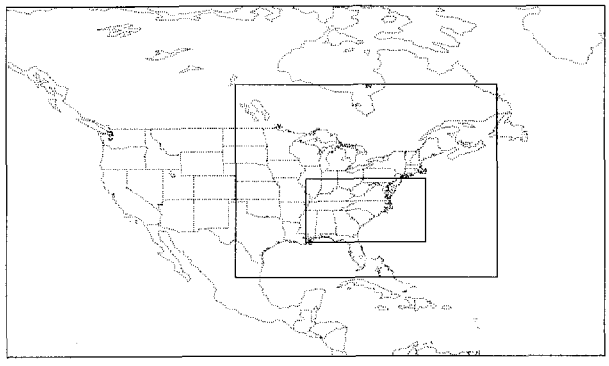

FIG. 6. The domain of the three NORAPS model horizontal nests as used in this study.

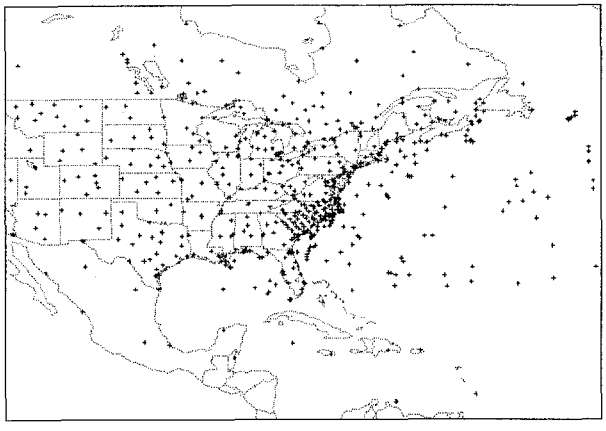

FIG. 8. Location of surface data stations within the objective analysis domain reporting at 0000 UTC 25 January 1986.

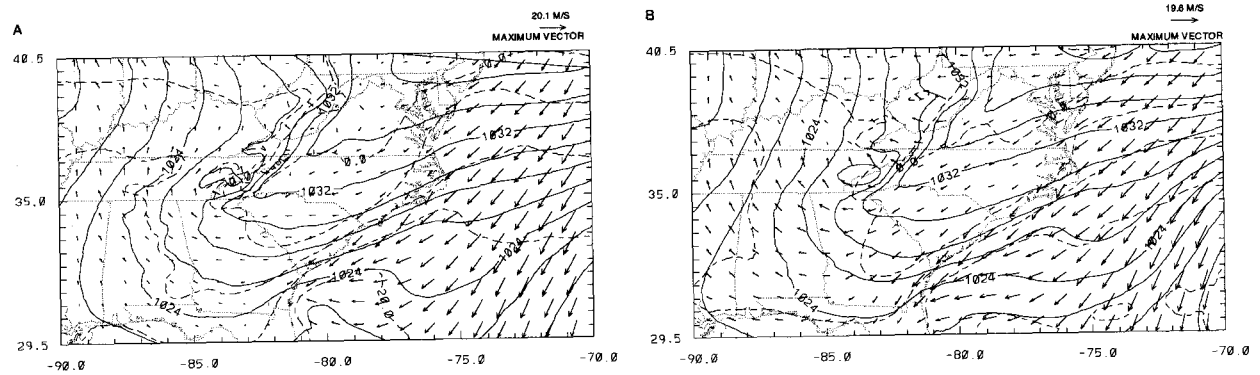

FIG. 9. Analyses of sea level pressure (solid contours), lowest sigma layer temperature (dashed contours), and wind vectors valid at 0000 UTC 25 January 1986 for (a) experiment 1 and (b) experiment 2. Temperature is contoured every 5°C, sea level pressure every 2 mb, and wind vectors are meters per second.

series of analyses for the IOP. High-resolution surface analyses were generated on a 20-km resolution grid. Lower-resolution surface and upper-air analyses were constructed over a 44-km resolution grid. DW used data from all the available sources during GALE and pursued rigorous quality control methods to rid the data of errors and systematic biases. In comparing the analyses and forecasts generated by the surface data assimilation with those of DW, emphasis is put on the positioning and strength of the coastal front. Because the coastal front is generated in part by differential surface diabatic heating (Bosart et al. 1972), it is an ideal feature to evaluate the impact of surface data assimilation in an analysis and forecast system. Coastal fronts are also an important feature to be able to forecast because they can have a large impact on the mesoscale location, amount, and phase of precipitation (Bosart et al. 1972; Marks and Austin 1979) and can, in some cases, have a sizable impact on the synoptic scale (Uccellini et al. 1987). Operational numerical weather prediction models have, in the past, had trouble forecasting the existence and strength of cold-air damming (Bell and Bosart 1988) as well as coastal frontogenesis. This has been due in part to the model's inability to reproduce some of the important physical mechanisms used to generate cold-air damming and coastal frontogenesis due to the limited horizontal and vertical model resolution used. However, high-resolution mesoscale models have been successfully used to simulate these phenomena (Ballentine 1980; Doyle and Warner 1993a,b).

4. Results

During this case study the NORAPS model had a general tendency to underforecast the strength of the cold-air damming in the short range 0–12-h forecasts considered here. This led to the model not retaining the proper location or gradient of the coastal front. The principal mechanisms for establishing and maintaining the cold-air damming are cold-air advection generated by a northerly low-level jet east of the Appalachian Mountains and evaporative cooling from precipitation aloft (Bell and Bosart 1988). Cold-air damming and coastal fronts are very shallow features (<1000 m) and it is possible that the configuration of the NORAPS model used here with 7 layers below 850 mb does not contain enough low-level vertical resolution for them compared to the 15 layers used below 850 mb by Doyle and Warner (1993a). A further reason for the forecast error is due to the boundary conditions generated by the intermediate grid for the inner grid. On the intermediate grid the horizontal resolution (about 50 km) is also probably not sufficient to generate the strong cold-air damming and northerly flow at the northern edge of the finest grid's domain. With this weaker damming on the intermediate grid, there is insufficient cold-air advection into the finest grid. Although the resolution problems can be corrected with increased vertical resolution and a larger domain for the finest inner grid, that is not the purpose here. Instead, given this model bias, the corrective influence of the surface data assimilation is readily assessed in this paper.

a. *Impact of assimilation of surface observations at synoptic times*

Figure 9 contains analyses of the lowest model level winds, temperature, and sea level pressure valid at 0000 UTC 25 January 1986 for experiments 1 (upper-air data only) and 2 (upper-air and surface data). The addition of the surface data enhances the low-level analysis in several ways. The thermal gradient from the developing coastal front off the North Carolina coast is better depicted with the inclusion of surface data. At this time the coastal front was still offshore (see DW Fig. 5a) in agreement with the surface data analysis, where the thermal gradient is closer to the coast and stronger than the upper-air data analysis. The surface data analysis also enhances the inverted high pressure

ridge in northern Virginia. The winds for the surface data analysis, particularly in South Carolina, contain more of a northerly component. All together the surface data analysis better depicts the detailed mesoscale features of the cold-air damming and coastal frontogenesis situation compared to the upper-air data analysis alone. Twelve hours later, at 1200 UTC 25 January, the convergence along the coastal front became more developed (see DW Fig. 5c). The surface data analysis for this time (not shown) improves the upper-air data analysis by correctly positioning the convergence zone and associated sea level pressure trough along the coast.

b. *Impact of the PBL adjustment procedure on analyses and model forecasts*

Figure 10 contains three profiles each of potential temperature in the lower troposphere for Beaufort, North Carolina (34.71°N, 76.67°W), and Petersburg, Virginia (37.18°N, 77.52°W). The profiles are 1) the 6-h model forecast that serves as the background, 2) observed soundings that were taken as part of the supplemental soundings during GALE, and 3) the profiles that result from the surface data analysis and PBL adjustment procedure. In Fig. 10a, the background sounding for Beaufort is more than 9 K warmer than the observation at the bottom level because of the incorrect placement of the coastal front that is located in the region. The surface data analysis is able to reduce the difference to slightly less than 4 K (the thermal gradient in the area was too tight for the analysis to fully resolve). If no further changes were made to the new three-dimensional analysis field, the result would have been a strong but extremely shallow stable layer. However, the PBL adjustment procedure allows for a much smoother vertical transition. The background and analysis profiles converge near the top of the boundary layer. The figure shows that not only does the analysis and adjustment procedure bring the mean potential temperature for the lower level closer to the observed, but in this case it also replicates the general stability of the lowest 50 mb. The profiles for Petersburg, which was well into the cold-air damming and away from the strong thermal gradient, are shown in Fig. 10b. Again, as in Fig. 10a, the low level of the observed sounding is cooler than the background profile. In this case, the surface data analysis matches almost exactly to the surface observation. The mean value of the lower-level profile is again brought closer to the observed sounding. However, for Petersburg, the general stability profile is not as well replicated as for Beaufort. Even with the adjustment procedure, the strongest stable layer remains near the surface.

The utility of the surface data analysis and PBL adjustment procedure can be seen in a broader context by looking at a comparison of vertical cross sections. Figure 11 contains cross sections of potential temperature and wind speed from Asheville, North Carolina (35.35°N, 82.47°W), to Cape Hatteras, North Carolina (35.27°N, 75.55°W), resulting from a 6-h model forecast valid at 0600 UTC 25 January 1986 and a surface data analysis and PBL adjustment for the same time. For comparison, Fig. 10b of DW is a cross section for the same horizontal domain based on five supplemental

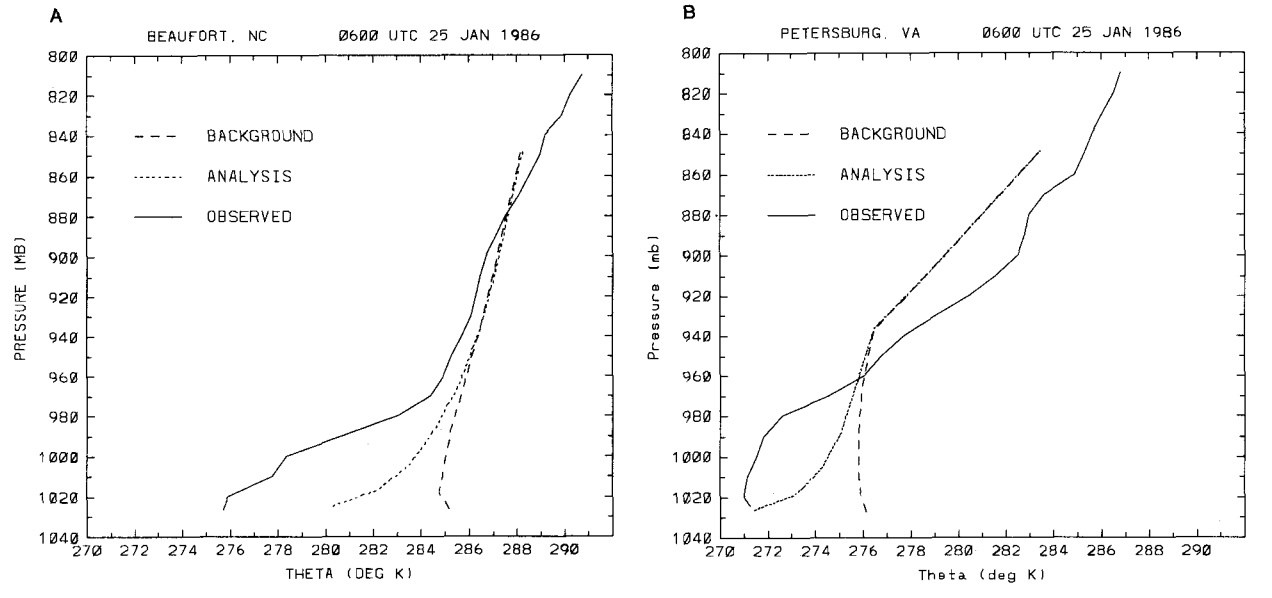

FIG. 10. Potential temperature (K) profiles in the lower troposphere valid at 0600 UTC 25 January 1986 for (a) Beaufort, North Carolina, and (b) Petersburg, Virginia. The observed profile (solid line) is from a radiosonde observation, the background profile (large dash line) from a 6-h forecast initialized at 0000 UTC and the analysis profile (small dash line) that results from the surface data analysis and the PBL adjustment procedure.

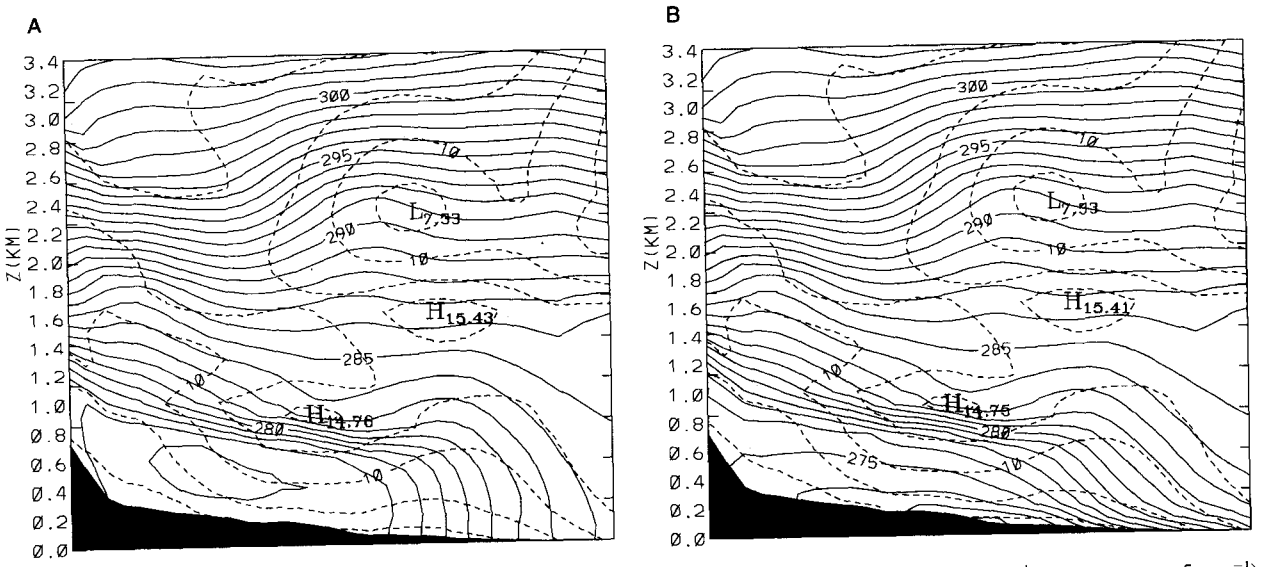

FIG. 11. Vertical cross sections of potential temperature (K; contours every 1 K) and vector wind speed (m s^{-1}; contours every 5 m s^{-1}) valid at 0600 UTC 25 January 1986 from a 6-h forecast initialized at 0000 UTC (a) and from the surface data analysis and PBL adjustment performed at 0600 UTC (b).

soundings available during GALE. The forecast cross section does show some cold-air damming although not as strong as indicated in DW. In the analysis cross section the magnitude of the cold-air dome is increased and the thermal gradient is pushed further toward the coast. Both of these changes bring the analysis closer to the observed cross section of DW. One problem with the analysis is that the slope of the isentropes over the surface front near Cape Hatteras should be steeper. This arises partly because the surface is cooler than the background's higher layers and the nudging toward the updated eddy diffusivities act to brake the vertical mixing of the deviations.

A reason for the implementation of the PBL adjustment procedure was to help merge the bottom model layer's surface data analysis with the rest of the first-guess fields. Preliminary testing revealed that many of the changes produced by the surface data analysis alone were lost though the initialization process. Because it would infer the presence of gravity waves, the initialization procedure would damp out the features the surface data analysis put in. To demonstrate that the PBL adjustment could alleviate this situation, the analysis in Fig. 9b was initialized without the adjustment procedure for experiment 2 (Fig. 12a) and with the adjustment procedure for experiment 3 (Fig. 12b). The initialization with the adjustment procedure retains more details of the surface data analysis thermal fields. It also has the least modification to the analysis wind fields, particularly to the west of the Appalachian mountains. Both initialization runs weaken the inverted ridging occurring east of the Appalachians. The utility of the PBL adjustment scheme can also be seen in the model forecasts. Figure 13 contains 12-h forecasts valid at 0000

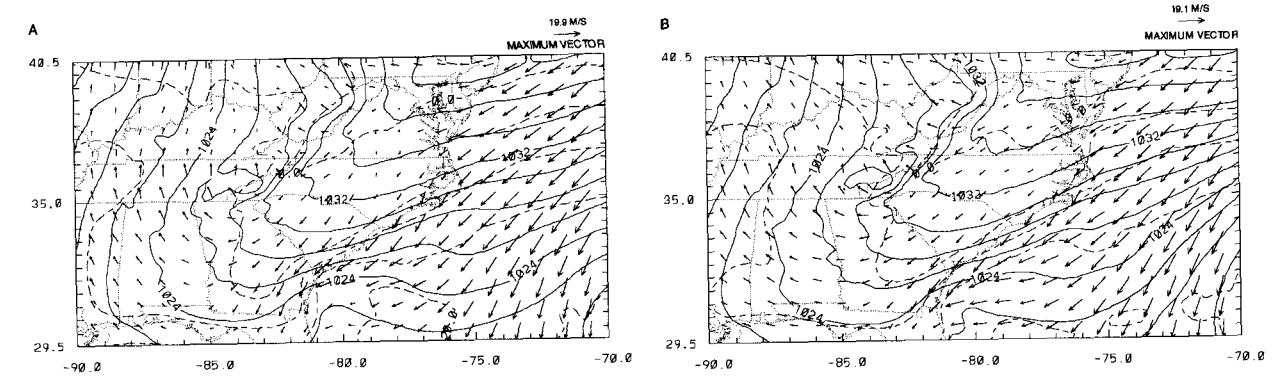

FIG. 12. Same as Fig. 9 except initialized fields (a) without and (b) with the PBL adjustment procedure.

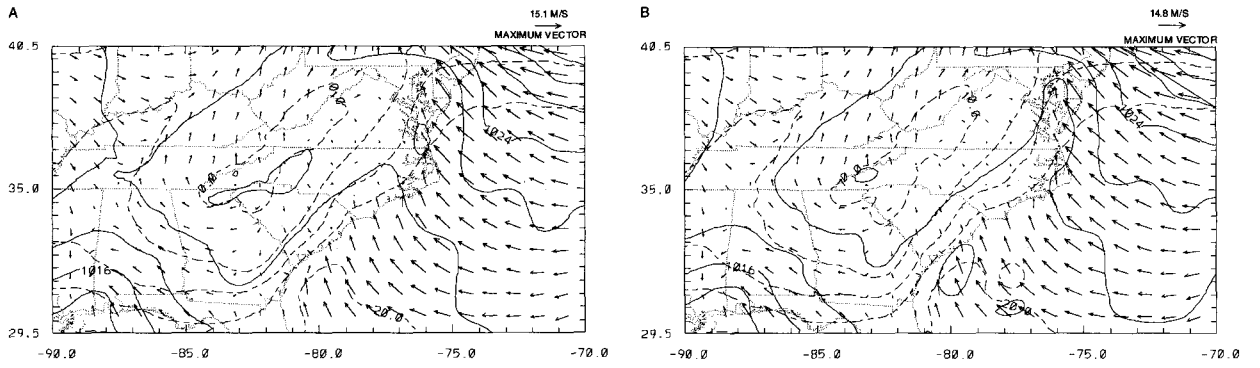

FIG. 13. Same as Fig. 9 except 12-h model forecasts valid at 0000 UTC 26 January 1986 from (a) experiment 2 and (b) experiment 3.

UTC 26 January 1986 for experiments 2 and 3. Although the forecast temperature and wind fields are similar for the two forecasts, the forecast with the PBL adjustment does a better job depicting the sea level pressure field. The experiment 3 forecast correctly shows the details of the inverted trough associated with the coastal front and the developing low off the Georgia and South Carolina coasts. Because sea level pressure is a vertically integrated quantity, it is reasonable that it would benefit from the PBL adjustment procedure.

c. *Impact of frequent assimilation of surface observations on analyses and model forecasts*

Surface forecasts that are valid at 1200 UTC 25 January 1986 are compared for the different assimilation cycles in Fig. 14. Figure 14a is the lowest-layer temperature and wind fields along with sea level pressure for a 12-h forecast from the 12-h assimilation cycle of experiment 3. Figure 14b contains the same fields for the latest 3-h forecast from the 12-h upper-air and 3-h surface data assimilation cycle in experiment 5. The experiment 5 forecast shows the benefit of the more frequent surface data assimilation in that it retains a tighter gradient near the coastal front and keeps the lower-level temperatures east of the Appalachian mountains colder. In addition, the experiment 5 forecast still retains the strong convergence along the South Carolina and Georgia coasts even though it has undergone three additional analysis and initialization steps. Both sea level pressure forecasts show the presence of a trough associated with the coastal front. However, the 3-h surface data assimilation forecast has a sharper trough and positions it closer to its observed position along the mid-Atlantic coast (see DW Fig. 5c). Overall, these results indicate that in a continuing data assimilation system, for a short-term forecast, it is beneficial to include the latest surface observations into a model even it there is no corresponding upper-air data.

It is interesting to see the impact that these differing forecasts have on the resultant lower-level analyses. Figure 15 is the result of the upper-air and surface data analysis at 1200 UTC 25 January using the 12-h forecast from Fig. 14a as the background. Figure 15b uses the forecast fields from the 3-h surface data assimilation cycle in Fig. 14b as the first guess in the analysis. Because the objective of an assimilation system is to blend the high-resolution features generated by the model with observed data, it should come as no surprise that the analysis that used the 3-h assimilation cycle forecast

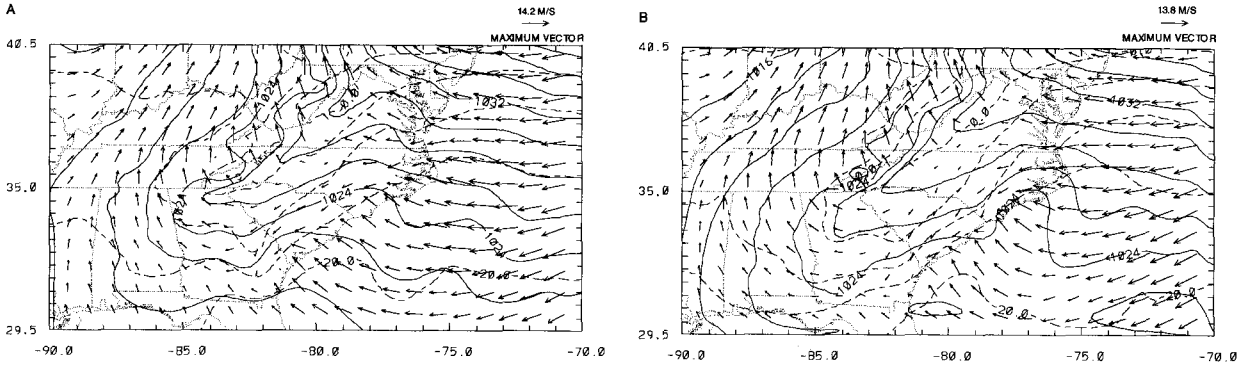

FIG. 14. Same as Fig. 9 except 12-h forecast from (a) experiment 3 and (b) 3-h forecast from experiment 5. Both forecasts are valid at 1200 UTC 25 January 1986.

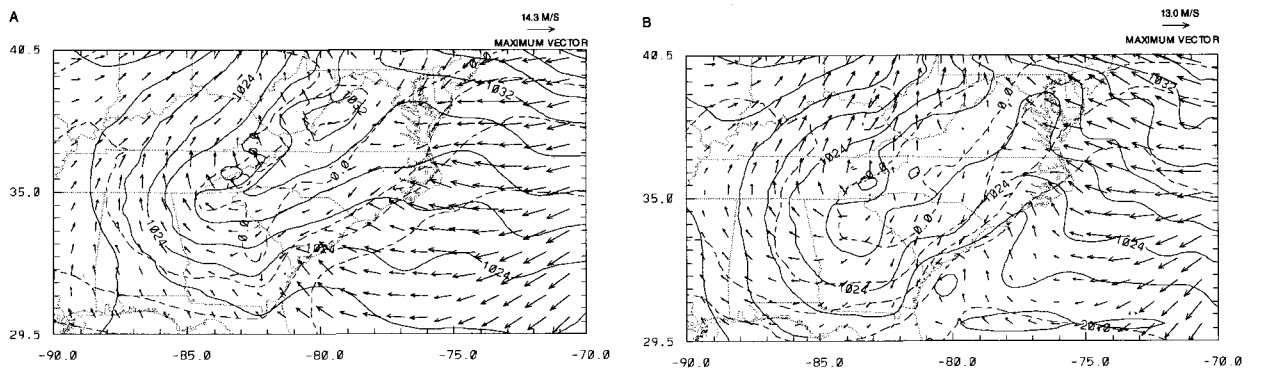

FIG. 15. Same as Fig. 9 except analyses valid at 1200 UTC 25 January 1986 for (a) experiment 3 and (b) experiment 5.

as background, with its tighter gradients and sharper features, is superior. The analysis from the 3-h assimilation cycle has a tighter thermal gradient along the coast, which the analysis moved slightly to the east from the first guess. It also retains the sharp inverted trough associated with the coastal front and positions it favorably compared to DW's analysis for the same time. The 12-h assimilation analysis has only a broad shallow trough that is placed too far east, off the North Carolina coast. One of the reasons that the 3-h assimilation results in a more detailed analysis than the 12-h assimilation is the effect of the error weighting described in section 3b. Because the 3-h assimilation analysis uses a 3-h forecast compared to a 12-h forecast, there is less forecast error growth, and thus the background field takes on more importance than in the 12-h assimilation.

Figure 16 contains forecasts ranging from 3 to 12 h, all initialized using the analysis from experiment 2 at 1200 UTC 25 January 1986. Figure 17 contains forecasts of the same lengths and valid times as Figure 16 but uses the analysis from experiment 5. For all the runs the forecasts initialized with the more frequent assimilated surface data show tighter thermal gradients for the front along the coast of the Carolinas. The differences in the gradients diminish over the length of the

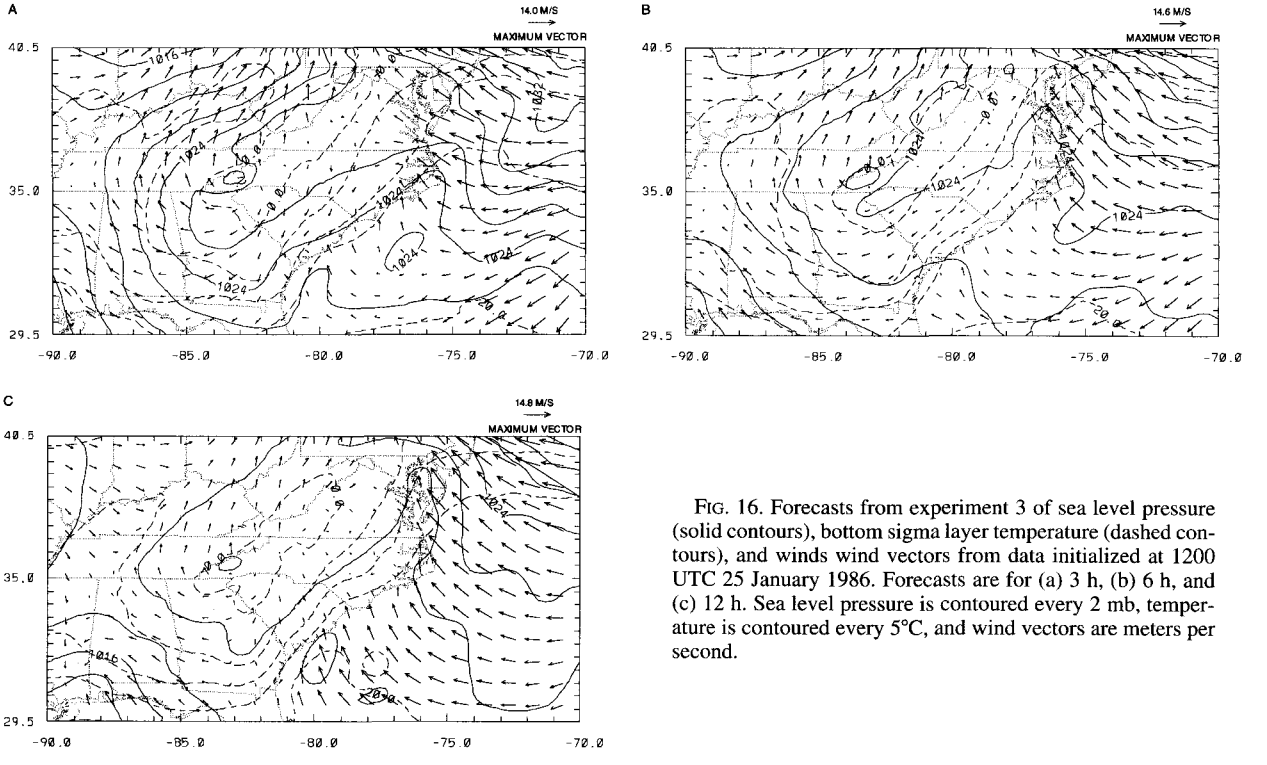

FIG. 16. Forecasts from experiment 3 of sea level pressure (solid contours), bottom sigma layer temperature (dashed contours), and winds wind vectors from data initialized at 1200 UTC 25 January 1986. Forecasts are for (a) 3 h, (b) 6 h, and (c) 12 h. Sea level pressure is contoured every 2 mb, temperature is contoured every 5°C, and wind vectors are meters per second.

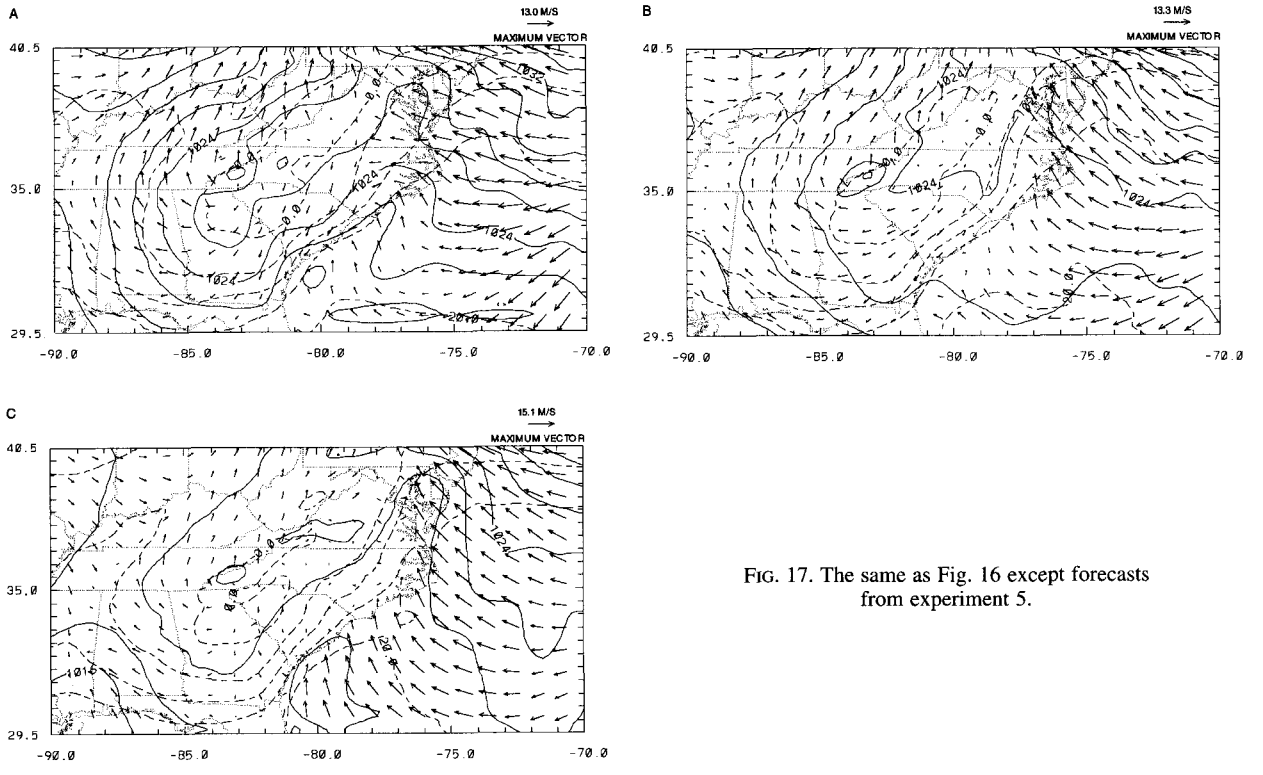

FIG. 17. The same as Fig. 16 except forecasts from experiment 5.

forecast. The inverted surface trough associated with the coastal front is more sharply defined by the experiment 5 forecast at 3 h (Fig. 17a). At 6 h (1800 UTC) the definition of the coastal trough is close for both forecasts but the experiment 5 forecast (Fig. 17b) positions the trough slightly further inland, which compares favorably to DW analysis (see DW Fig. 5d). Although not perfectly accurate in the position, the temperature pattern in Fig. 17b for the experiment 5 forecast indicates the existence of a wave along the front in North Carolina. By 12 h, the advantage of having assimilated the surface data every 3 h is less noticeable.

Comparison of surface data analysis with and without PAMS data (not shown) revealed that the high spatial density PAMS data had little effect. This occurred because the PAMS data density (50 km) is approximately the same as the surface data analysis grid. As detailed by Koch et al. (1983), an ideal ratio between analysis grid and observational spacing is 0.3–0.5. Although the analysis resolution could have been increased for the PAMS data, it would have required that the model's inner grid resolution be also increased to provide sufficient resolution for the background field. This would have caused problems regarding the hydrostatic assumption and some of the model's physical parameterizations. The effect of the frequent data assimilation on the model's coarser ($\Delta x \approx 50$ km) intermediate grid can be seen in Fig. 18, which contains 6-h forecasts valid at 1800 UTC 25 January from experiments 3 and 5. Over North America, the forecasts are practically identical, with differences of contour line positions of only a grid point or so. The surface data analysis is most likely identifying features that are too small to be resolved by the intermediate grid. This probably is exacerbated by the presence of a horizontal diffuser in the model.

5. Conclusions

A system for intermittent assimilation of asynoptic surface observations using a mesoscale model has been presented. After making adjustments to the observations to account for model and observation height differences, an objective analysis step on the model's lowest sigma layer is carried out. Once the bottom model layer is updated, the deviations from the model background field at that level are blended vertically within the boundary layer. The vertical distribution of the deviations is accomplished by a physically based PBL adjustment scheme that uses the model's values of eddy diffusivity that are nudged to reflect the updated values. In the case study presented here, the PBL adjustment scheme was shown to have a beneficial impact when combining upper-air and surface data in a 12-h assimilation update cycle. A 3-h surface data analysis and PBL adjustment assimilation cycle, coupled with upper-air data assimilated every 12 h, yielded better anal-

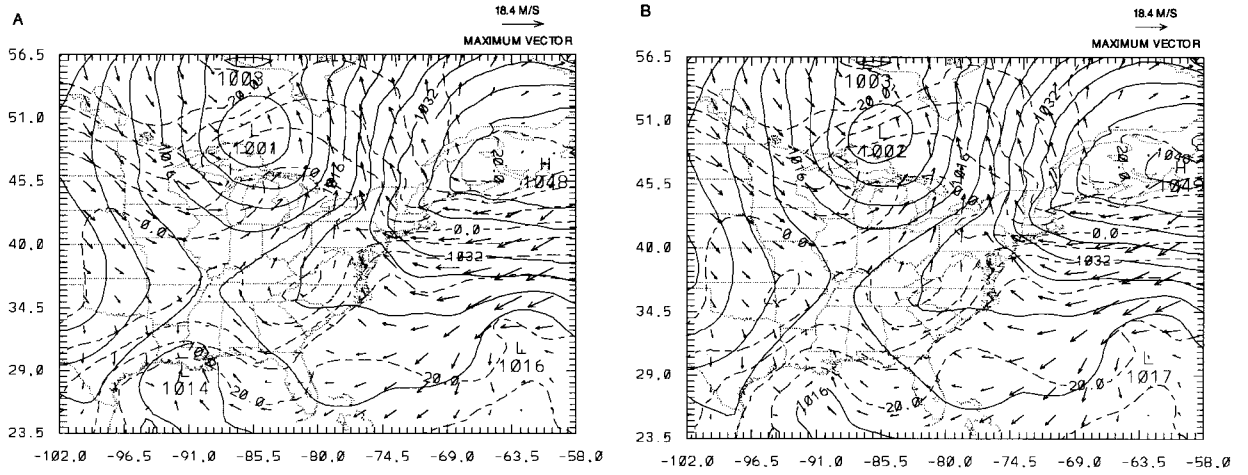

FIG. 18. Six-hour forecasts of sea level pressure (mb; contoured every 4 mb), lowest model layer temperature (°C; contoured every 5°C) and wind vectors (m s^{-1}) on 1.5° resolution intermediate model grid valid at 1800 UTC 25 January 1986 for (a) experiment 3 and (b) experiment 5.

yses and forecasts in the 3–12-h range compared to analyses and forecasts that used only 12-h assimilated upper-air and surface data. The impact of the frequent surface data assimilation dissipates for larger model grid spacing. The improvement in analyses and forecasts come about from better resolution of mesoscale features. Improved short-term forecasts can be achieved by continuing to assimilate surface data beyond the traditional synoptic cutoff times. The results suggest that as model resolution increases, the beneficial impact of including high-resolution data sources will increase. It is possible, given the results here that in an operational setting at a local forecast office, limitations imposed on the physics and resolution of a mesoscale model can be overcome through the use of the FDDA of asynoptic surface observations. Extrapolation of the results presented here would indicate that other two-dimensional data sources can be useful in FDDA as long as there is reasonable method for blending the data into the third dimension. Future improvements to the technique will involve increasing the sophistication of the PBL adjustment procedure by using the temporal evolution of the PBL during background forecast period and updating.

Acknowledgments. Computer time for this work was provided by the Naval Research Laboratory Central Computer Facility. The authors thank Donald A. Chisholm, Samuel Y. K. Yee, and George D. Modica for their helpful suggestions on improving this manuscript.

REFERENCES

Arakawa, A., and V. R. Lamb, 1977: Computational design of the basic dynamical processes of the UCLA general circulation model. *General Circulation Models of the Atmosphere,* J. Chang, Ed., *Methods in Computational Physics, Vol. 17,* Academic Press, 173–265.

Ballentine, R. J., 1980: A numerical investigation of New England coastal frontogenesis. *Mon. Wea. Rev.,* **108,** 1479–1497.

Barwell, B. R., and A. C. Lorenc, 1985: A study of the impact of aircraft wind observations on a large-scale analysis and numerical weather prediction system. *Quart. J. Roy. Meteor. Soc.,* **111,** 103–129.

Bell, G. D., and L. F. Bosart, 1988: Appalachian cold-air damming. *Mon. Wea. Rev.,* **116,** 137–161.

Benjamin, S. G., 1989: An isentropic mesoα-scale analysis system and its sensitivity to aircraft and surface observations. *Mon. Wea. Rev.,* **117,** 1586–1603.

——, and P. A. Miller, 1990: An alternative sea level pressure reduction and a statistical comparison of geostrophic wind estimates with observed surface winds. *Mon. Wea. Rev.,* **118,** 2099–2116.

——, K. A. Brewster, R. L. Brümmer, B. R. Jewett, T. W. Schlatter, T. L. Smith, and P. A. Stamus, 1991: An isentropic three-hourly assimilation system using ACARS aircraft observations. *Mon. Wea. Rev.,* **119,** 888–906.

——, K. J. Brundage, P. A. Miller, T. L. Smith, G. A. Grell, D. Kim, J. A. Brown, and T. A. Schlatter, 1994: The rapid update cycle at NMC. Preprints, *10th Conf. on Numerical Weather Prediction,* Portland, OR, Amer. Meteor. Soc., 566–568.

Blackadar, A. K., 1979: High resolution models of the planetary boundary layer. *Advances in Environmental Science and Engineering, Vol. 1,* J. R. Pfallin and E. N. Ziegler, Eds. Gordon and Breach, 50–85.

Bosart, L. F., C. J. Vaude, and J. H. Helsdon Jr., 1972: Coastal frontogenesis. *J. Appl. Meteor.,* **11,** 1236–1258.

Bourke, W., and J. L. McGregor, 1983: A nonlinear vertical mode initialization scheme for a limited area prediction model. *Mon. Wea. Rev.,* **111,** 2285–2297.

Bratseth, A. M., 1986: Statistical interpolation by means of successive corrections. *Tellus,* **38A,** 439–447.

Charney, J., M. Halem, and R. Jastrow, 1969: Use of incomplete historical data to infer the present state of the atmosphere. *J. Atmos. Sci.,* **26,** 1160–1163.

Cotton, W. R., G. Thompson, and P. W. Mielke Jr., 1994: Real-time mesoscale predictions on workstations. *Bull. Amer. Meteor. Soc.,* **75,** 349–362.

Daley, R., 1991: *Atmospheric Data Analysis.* Cambridge University Press, 457 pp.

Davies, H. C., 1976: A lateral boundary formulation for multilevel prediction models. *Quart. J. Roy. Meteor. Soc.,* **102,** 408–418.

Detering, H. W., and D. Etling, 1985: Application of the E-ϵ turbulence model to the atmospheric boundary layer. *Bound.-Layer Meteor.*, **33,** 113–133.

DiMego, G. J., 1988: The National Meteorological Center regional analysis system. *Mon. Wea. Rev.*, **116,** 977–1000.

——, K. E. Mitchell, R. A. Petersen, J. E. Hoke, and J. P. Gerrity, 1992: Changes to NMC's Regional Analysis and Forecast System. *Wea. Forecasting,* **7,** 185–197.

Doyle, J. D., and Warner, T. T., 1990: Mesoscale coastal processes during GALE IOP 2. *Mon. Wea. Rev.*, **118,** 283–308.

——, and ——, 1993a: A numerical investigation of coastal frontogenesis and mesoscale cyclogenesis during GALE IOP 2. *Mon. Wea. Rev.*, **121,** 1048–1077.

——, and ——, 1993b: Nonhydrostatic simulations of coastal mesobeta-scale vortices and frontogenesis. *Mon. Wea. Rev.*, **121,** 3371–3392.

Friday, E. W., Jr., 1994: The modernization and associated restructuring of the National Weather Service: An overview. *Bull. Amer. Meteor. Soc.*, **75,** 43–52.

Harms, D. E., S. Raman, and R. V. Madala, 1992a: An examination of four-dimensional data-assimilation techniques for numerical weather prediction. *Bull. Amer. Meteor. Soc.*, **73,** 425–440.

——, K. D. Sashegyi, R. V. Madala, and S. Raman, 1992b: Four dimensional data assimilation of GALE data using a multivariate analysis scheme and mesoscale model with diabatic initialization. NRL Memo. Rep. 7147, Naval Research Laboratory, Washington D.C., 219 pp. [NTIS A256063.]

Harshvardhan, R. Davies, D. Randall, and T. Corsetti, 1987: A fast radiation parameterization for atmospheric circulation models. *J. Geophys. Res.*, **92,** 1009–1015.

Hodur, R. M., 1987: Evaluation of a regional model with an update cycle. *Mon. Wea. Rev.*, **115,** 2707–2718.

Kanamitsu, M., 1989: Description of the NMC Global Data Assimilation and Forecast System. *Wea. Forecasting,* **4,** 335–342.

Koch, S. E., M. Desjardins, and P. J. Kocin, 1983: An interactive Barnes objective map analysis scheme for use with satellite and conventional data. *J. Climate Appl. Meteor.*, **22,** 1487–1503.

Kuo, H.-L., 1974: Further studies of the influence of cumulus convection on large scale flow. *J. Atmos. Sci.*, **31,** 1232–1240.

Liou, C.-S., C. H. Walsh, S. M. Heikkinen, and R. L. Elsberry, 1990: Numerical studies of cyclogenesis events during the second intensive observation period (IOP-2) of GALE. *Mon. Wea. Rev.*, **118,** 218–233.

——, R. M. Hodur, and R. H. Langland, 1994: Navy Operational Atmospheric Prediction System (NORAPS): A triple nested mesoscale model. Preprints, *10th Conf. on Numerical Weather Prediction,* Portland, OR, Amer. Meteor. Soc., 423–425.

Louis, J. F., 1979: A parametric model of vertical eddy fluxes in the atmosphere. *Bound.-Layer Meteor.*, **17,** 187–202.

Madala, R. V., 1981: Efficient time integration schemes for atmosphere and ocean models. *Finite Difference Techniques for Vectorized Fluid Dynamic Calculations,* D. L. Book, Ed., Springer Verlag, 56–74.

——, S. W. Chang, U. C. Mohanty, S. C. Madan, R. K. Paliwal, V. B. Sarin, T. Holt, and S. Raman, 1987: Description of the Naval Research Laboratory limited area dynamical weather prediction model. NRL Memo. Rep. 5992. Naval Research Laboratory, Washington, D.C., 132 pp. [NTIS A182780.]

Manabe, S., J. Smagorinsky, and R. F. Strickler, 1965: Simulated climatology of a general circulation model with a hydrologic cycle. *Mon. Wea. Rev.*, **93,** 769–798.

Manobianco, J., L. W. Uccellini, K. F. Brill, and P. J. Kocin, 1991: Contrasting the impact of dynamic data assimilation on the numerical simulations of cyclogenesis during GALE IOP 10 and IOP 1. *Meteor. Atmos. Phys.*, **45,** 41–63.

Marks, F. D., Jr., and P. M. Austin, 1979: Effects of the New England coastal front on the distribution of precipitation. *Mon. Wea. Rev.*, **107,** 53–67.

McGinley, J. A., S. C. Albers, and P. A. Stamus, 1991: Validation of a composite convective index defined by a real-time local analysis system. *Wea. Forecasting,* **6,** 337–356.

Miller, P. A., and S. G. Benjamin, 1992: A system for the hourly assimilation of surface observations in mountainous and flat terrain. *Mon. Wea. Rev.*, **120,** 2342–2359.

Perkey, D. J., and C. W. Kreitzberg, 1976: A time-dependent lateral boundary scheme for limited-area primitive equation models. *Mon. Wea. Rev.*, **104,** 1513–1526.

Riordan, A. J., 1990: Examination of the mesoscale features of the GALE coastal front of 24–25 January 1986. *Mon. Wea. Rev.*, **118,** 258–282.

Robert, A. J., 1966: The investigation of a low order spectral form of the primitive meteorological equations. *J. Meteor. Soc. Japan,* Ser. 2, **44,** 237–245.

Sashegyi, K. D., and R. V. Madala, 1993: Application of vertical-mode initialization to a limited-area model in flux form. *Mon. Wea. Rev.*, **121,** 207–220.

——, D. E. Harms, R. V. Madala, and S. Raman, 1993: Application of the Bratseth scheme for the analysis of GALE data using a mesoscale model. *Mon. Wea. Rev.*, **121,** 2331–2350.

——, R. V. Madala, D. E. Harms, and S. Raman, 1994: A numerical weather prediction system for regional and mesoscale forecasting on a high performance workstation. Preprints, *10th Conf. on Numerical Weather Prediction,* Portland, OR, Amer. Meteor. Soc., 363–365.

Snook, J. S., J. M. Gram, and J. M. Schmidt, 1994: The "P" in LAPS: A local scale operational forecast system. Preprints, *10th Conf. on Numerical Weather Prediction,* Portland, OR, Amer. Meteor. Soc., 454–456.

Stauffer, D. R., and N. L. Seaman, 1990: Use of four-dimensional data assimilation in a limited-area mesoscale model. Part I: Experiments with synoptic-scale data. *Mon. Wea. Rev.*, **118,** 1250–1277.

Stull, R. B., 1988: *An Introduction to Boundary Layer Meteorology.* Kluwer Academic Publishers, 666 pp.

Tiedtke, M., W. A. Heckley, and J. Slingo, 1988: Tropical forecasting at ECMWF: The influence of physical parameterization on the mean structure of forecasts and analysis. *Quart. J. Roy. Meteor. Soc.*, **114,** 639–664.

Uccellini, L. W., R. A. Peterson, K. F. Brill, P. J. Kocin, and J. J. Tuccillo, 1987: Synergistic interactions between an upper-level jet streak and diabatic processes that influence the development of a low level jet and a secondary coastal cyclone. *Mon. Wea. Rev.*, **115,** 2227–2261.

Walko, R. L., C. J. Tremback, and W. R. Cotton, 1989: Assimilation of Doppler radar wind data into a numerical prediction model: A demonstration of certain hazards. Preprints, *24th Conf. on Radar Meteor.,* Tallahassee, FL, Amer. Meteor. Soc., 248–250.

Warner, T. T., and N. L. Seaman, 1990: A real-time mesoscale numerical weather-prediction system for research, teaching, and public service at Pennsylvania State University. *Bull. Amer. Meteor. Soc.*, **71,** 792–805.

Yee, S. Y. K., and A. J. Jackson, 1988: Blending of surface and rawinsonde data in mesoscale objective analysis. AFGL Tech. Rep. 88-0144, Air Force Geophysics Laboratory, Hanscom AFB, Massachusetts, 31 pp. [NTIS ADA203984.]